Plasmon-Assisted Resonant Electron Tunneling in a Scanning Tunneling Microscope Junction

Shuyi Liu,[1] Martin Wolf,[1] and Takashi Kumagai[1,2*]

[1]*Department of Physical Chemistry, Fritz-Haber Institute of the Max-Planck Society, Faradayweg 4-6, 14195 Berlin, Germany*
[2]*JST-PRESTO, 4-1-8 Honcho, Kawaguchi, Saitama 332-0012, Japan*

We report plasmon-assisted resonant electron tunneling from a Ag or Au tip to field emission resonances (FERs) of a Ag(111) surface induced by cw laser excitation of a scanning tunneling microscope (STM) junction at visible wavelengths. As a hallmark of the plasmon-assisted resonant tunneling, we observe a downshift of the first peak in the FER spectra by a fixed amount equal to the incident photon energy. STM-induced luminescence measurement for the Ag and Au tip reveals the clear correlation between the laser-induced change in the FER spectra and the plasmonic properties of the junction. Our results clarify a novel resonant electron transfer mechanism in a plasmonic nanocavity.

Plasmon-induced phenomena have attracted increasing attention due to diverse applications in nanoscale science and technology [1]. Plasmonic nanocavities play a particularly important role because of their ability to confine light to nanometric volumes and generate a strong field enhancement. In order to elucidate underlying physical mechanisms, it is essential to investigate the plasmon-induced processes in well-defined nanocavities with precise control of the separation distance. STM combined with optical excitation is a suitable method to examine light-induced processes in nanocavities [2]. In addition, the light-induced field enhancement and electron transfer (rectification) in STM junctions are of great interest as they are a key to realize ultrasensitive spectroscopy at the nanoscale down to the single-molecule level [3–6] and even with ultrahigh temporal resolution [7–14].

The interplay between plasmon response and electron transfer is intimately related to various applications such as photovoltaics, fast electronics, enhanced photochemistry, and plasmonic catalysis [1], where resonant electron transfer in plasmonic nanocavities is of fundamental importance. Light-assisted electron tunneling into a molecular resonance in a STM junction has been proposed previously [15,16] and this electron transfer could be enhanced through surface plasmon excitation. More recently, tip-enhanced Raman spectroscopy at low temperatures has opened up a new opportunity to investigate the plasmonic properties in the STM junction [4]. In this Letter, we report plasmon-assisted resonant tunneling in the junction consisting of a Ag or Au tip and a Ag(111) surface using the STM equipped with *in situ* optics for focusing and collecting light. The resonant tunneling occurs through the field emission resonances (FERs) in the junction which appear as multiple peaks in scanning tunneling spectroscopy (STS) [17,18]. This Rydberg-like series of the electronic states serves as a simple model to examine resonant electron transfer in the plasmonic nanocavity.

The experiments were performed in an ultrahigh vacuum (UHV) chamber (base pressure $<5 \times 10^{-10}$ mbar) equipped with a low-temperature STM (modified UNISOKU USM-1400) operated with a Nanonis SPM controller. The tip is fixed and the sample stage is equipped with the coarse motions (XYZ) and the tube piezo for scanning. All measurements were conducted at 78 K. A chemically etched Au or Ag tip was used (the Ag tip was supplied by UNISOKU Ltd.). The tips were cleaned by Ar^+ sputtering before measurement. The bias voltage was applied to the sample with the tip at ground. The Ag(111) surface was cleaned by repeated cycles of Ar^+ sputtering and annealing up to 670 K. The UHV chamber has fused silica windows for optical access. A cw laser (446 nm: laser diode, 532 nm: solid state laser, 633 nm: HeNe laser) was focused to the STM junction using an *in situ* Ag-coated parabolic mirror (numerical aperture of $\sim$0.6) mounted on the cold STM stage. The beam spot diameter on the tip apex was estimated to be about 3 μm. Accurate beam alignment and focusing were performed with piezo motors (attocube GmbH) attached to the parabolic mirror which allow three translational and two rotational motions. The polarization of the incident beam was parallel to the tip axis if not stated otherwise. The emitted light from the STM junction was collected by the parabolic mirror and detected outside of the UHV chamber with a grating spectrometer (AndorShamrock 303i). The STS (dI/dV) spectra were recorded using a lock-in amplifier with 20 mV modulation at 983 Hz, which is substantially faster than the STM feedback bandwidth. Illumination of the STM junction led to thermal expansion; however, the

226802-1

feedback loop ensured to avoid a crush of the junction and it did not cause any damage on the surface. The junction was equilibrated in ∼30 min after starting illumination and all STS data were measured under stationary conditions. In addition, a small thermal drift did not affect the STS spectra since the measurements were conducted with the STM feedback turned on (so-called constant current mode) and thus the drift was compensated by the feedback loop. Therefore, the thermal expansion and drift play a negligible role.

Figure 1(a) shows the STS spectra (solid curves) of a Ag tip-Ag(111) junction with and without 633-nm excitation ($h\nu = 1.96$ eV). The multiple peaks correspond to the series of the FERs which have been studied previously in the absence of illumination [19,20]. Under illumination the FER peaks are largely shifted to lower voltages and remarkably, the shift of the first FER peak (∼1.9 V) is nearly identical to the incident photon energy. Hereafter we denote the FER peaks by n and $n'(= 1, 2, 3, ...)$ for the case without and with illumination, respectively. Note that the STS spectra were recorded in the constant current mode which allows us to measure a wide voltage range, but leads to a continuous increase of the tip-surface distance with increasing the bias voltage [see dashed lines in Fig. 1(a)] [17]. Figure 1(b) shows the dependence of the FER spectra on the incident power density. It can be seen that the $n'(n) = 1$ peak at ∼2.2(∼ 4.2) V grows (diminishes) as the power density increases.

It was found that the downshift of the $n' = 1$ peak shows a clear correlation with the incident photon energy. As seen in Fig. 1(c), when the junction was illuminated with the 532-nm laser ($h\nu = 2.33$ eV), the $n' = 1$ peak was shifted by ∼2.3 V relative to $n = 1$. Furthermore, it was shifted by ∼2.8 V with the 446-nm laser ($h\nu = 2.78$ eV, see Supplemental Material [21]).

We also found that plasmonic properties of the STM junction correlate with the light-induced change of the FER peaks. Figures 2(a) and 2(b) show the STM-induced luminescence (STML) and the FER spectra, respectively, measured for a Au and Ag tip-Ag(111) junction. The STML intensity is much higher for the Ag tip than Au most probably due to the weak plasmon damping of Ag. The cutoff wavelength of the STML (plasmon excitation) is determined either by the quantum cutoff [19] that is simply the applied bias voltage ($V_s = 3$ V) or by the interband transition that is ∼4 eV (∼310 nm) and ∼2.5 eV (∼496 nm) for Ag and Au, respectively [22]. In Fig. 2(a), the cutoff wavelength of the Ag and Au tip corresponds to the former and latter case, respectively. Figure 2(b) displays the FER spectra obtained for a Au and Ag tip under 532-nm excitation with the same incident power density (0.10 mW/μm^2). The light-induced change is observed only for the Ag tip. Even at a high power density, no change occurs for the Au tip (see Supplemental Material [21]). However, the similar change occurs for the
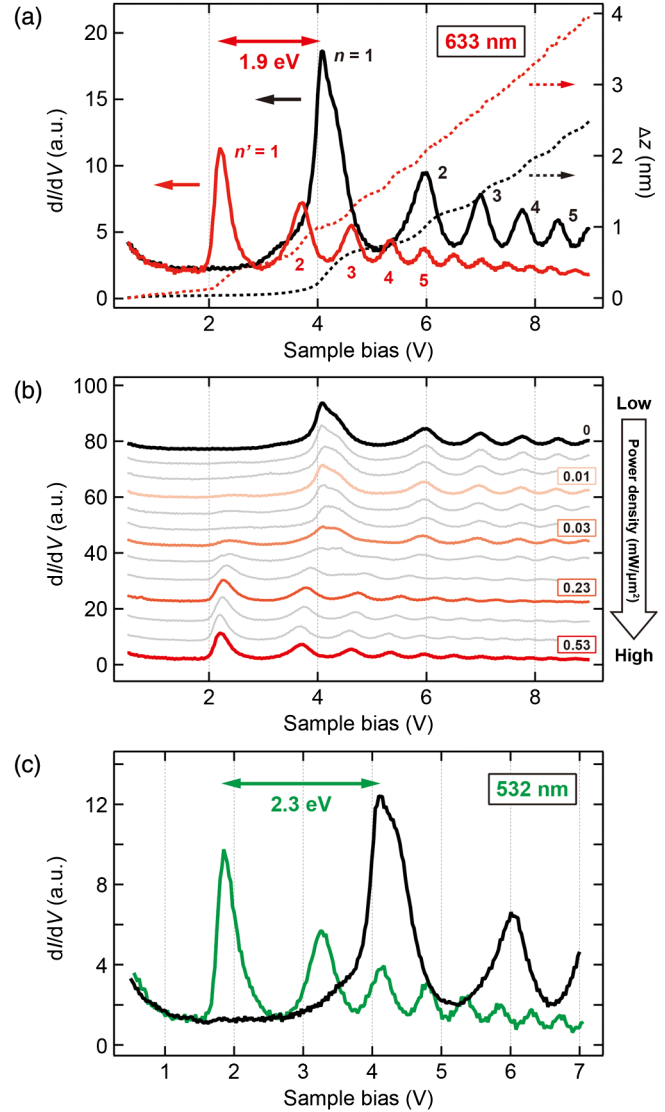

FIG. 1. (a) FER spectra (solid curves, left axis) of a Ag tip–Ag(111) surface junction with (red) and without (black) 633-nm excitation ($h\nu = 1.96$ eV). The junction is illuminated with a power density of 0.53 mW μm^{-2}. The spectra were recorded in the constant current mode at 0.1 nA. The tip-sample vertical displacements (Δz) are also plotted (dashed curves, right axis). (b) Incident power dependence of the FER spectra. The power density is varied from 0 to 0.53 mW μm^{-2}. The spectra are vertically offset for clarity. (c) FER spectra of a Ag tip-Ag(111) surface junction with (red) and without (black) 532-nm excitation ($h\nu = 2.33$ eV). The junction is illuminated at a power density of 0.84 mW μm^{-2}. The spectra were recorded in the constant current mode at 0.1 nA.

Au tip with 633-nm excitation [cf. Fig. 3(a)]. The STML spectrum, i.e., the plasmonic properties of the STM junction, is also sensitive to the tip shape [23]. We also examined the impact of the tip shape on the light-induced change of the FER spectra (see Supplemental Material [21]). In addition, the light-induced change strongly depends on
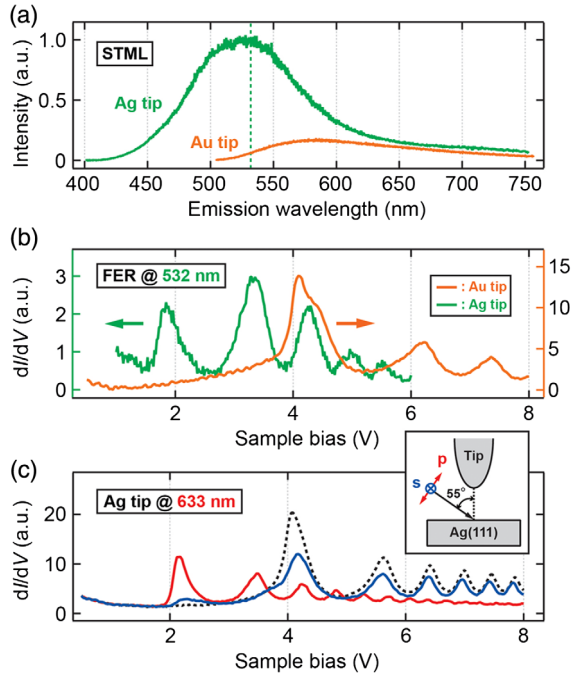
FIG. 2. (a) STML spectra measured over the Ag(111) surface with a Au (orange) and Ag (green) tip ($V_s = 3$ V, $I_t = 9$ nA). The vertical green broken line indicates the excitation wavelength in the FER measurement (532 nm). (b) FER spectra of a Au (orange) or Ag (green) tip-Ag(111) surface junction under 532-nm excitation with a power density of 0.10 mW μm^{-2}. The spectra were recorded in the constant current mode at 0.1 nA. (c) Polarization dependence of the FER spectra for a Ag tip-Ag (111) junction under 633-nm illumination with an incident power density of 0.09 mW/μm^2. The red, blue, and black broken lines correspond to the p polarization, s polarization, and nonilluminated cases, respectively. The inset shows schematic of the experimental geometry.

the polarization of the incident beam. When the incident beam is linearly polarized parallel to the tip axis (p polarized), the change is much larger than that for the polarization perpendicular to the tip axis (s polarized). These results clearly indicate that the light-induced process is governed by the field enhancement through surface plasmon excitation. The incident beam spot of ~3 μm is significantly larger than the very apex of the tip. Therefore, the field enhancement in the junction may result not only from a localized surface plasmon resonance at the apex but also from propagating surface plasmon polaritons launched on the tip shaft. The latter may lead to accumulation of the field enhancement at the apex through the adiabatic nanofocusing effect [24,25].

The assignment of the $n' = 1$ peak to the first FER state appears straightforward from the unequivocal correlation of the downshift by a fixed amount equal to the incident photon energy relative to $n = 1$. In order to assign the higher-order peaks ($n' \geq 2$), we performed FER intensity mapping at the respective peak voltages with and without

illumination. This measurement was carried out using a Au tip with 633-nm excitation. Figure 3(a) shows the FER spectra recorded for a Au tip-Ag(111) surface. The FER signal is sensitive to local structures or defects of the surface which cause a modulation of local electronic states and work functions [20,26–29]. Figure 3(b) shows the topographic image of the measurement area that includes a monoatomic step and an intrinsic defect on Ag(111). Figures 3(c)–3(e) display the FER intensity maps at $n = 2$, 3, 4 peaks [labeled by (c),(d),(e) in Fig. 3(a)]. In the defect, a unique feature of the FER state is observed, which differs at the respective FER voltages. Figures 3(f)–3(h) show the maps at $n' = 2$, 3, 4 peaks under 633-nm illumination [labeled by (f),(g),(h) in Fig. 3(a)]. The FER intensity distributions are very similar at the same ordinal number of the peaks with and without illumination. Therefore, we can assign unambiguously the peaks (f),(g),(h) in Fig. 3(a) to the second, third, and fourth FER states.

Figure 4 illustrates the energy diagram of the STM junction including the FERs along with schematic electron wave functions. FERs are quantized standing-wave states that have a maximum probability density in front of the surface. Here we assume a single particle picture with a simple one-dimensional potential introduced by Chulkov et al. [30] which is deformed by the applied bias voltage in the junction. Without illumination [Fig. 4(a)] the FER peaks appear when the bias voltage matches the respective resonances, $V_{n=1,2,3...}$ at which the electrons at the Fermi level of the tip are transferred to the corresponding FER state. As the field enhancement becomes substantially large, the plasmon-assisted tunneling takes place [Fig. 4(b)] and the bias voltages of the FER peaks downshift to $V_{n'=1,2,3...}$ at which the electrons at the Fermi level of the tip are resonantly excited and transferred to the FER state.

In Fig. 1(b), it can be seen that the threshold power density at which the plasmon-assisted tunneling occurs is higher for the higher-order FERs. This is explained either by the reduction of the field enhancement and/or by a wider tunneling barrier in the junction, resulting from the increase of the tip-surface distance at the higher voltages [as explained in Fig. 1(a)]. The field enhancement in the nanoscale junction decays rapidly within a few nm range [31]. The plasmon-assisted and "normal" STM tunneling processes compete with each other. This is observed at intermediate incident power densities in Fig. 1(b) (e.g., at 0.03 mW/μm^2), where the $n = 1$ and $n' = 1$ peaks appear at ~2.2 and ~4.2 V, respectively. However, the normal STM tunneling into the FERs becomes negligible when the plasmon-assisted tunneling is dominant since the tip-surface separation becomes large.

Previous studies suggest that the peak position of the first FER state is sensitive to the change in the local work function [27,28,32,33]. In Fig. 1(b), the $n' = 1$ peak position is shifted only slightly as the incident power density increases. We attribute this small change to an
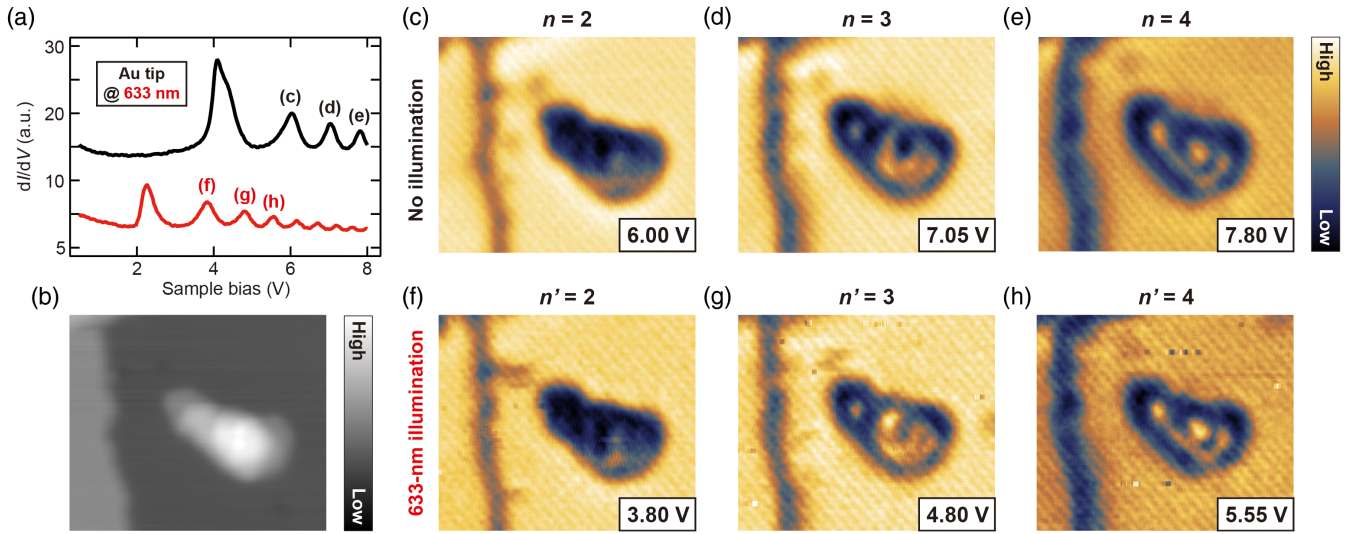
FIG. 3.   (a) FER spectra of a Au tip-Ag(111) surface junction with (red) and without (black) 633-nm excitation. The latter is vertically offset for clarity. The spectra were recorded in the constant current mode at 0.1 nA. The power density was set to 0.20 mW μm^{-2}. (b) Topographic image of the Ag(111) surface with a monoatomic step and an intrinsic defect ($V_s = 1$ V, $I_t = 0.1$ nA, 10×12 nm^2). (c)–(e) FER mapping at different bias voltages (indicated in the figure) without laser excitation. (f)–(h) FER mapping at different bias voltages (indicated in the figure) with laser excitation (illuminated with a power density of 0.20 mW μm^{-2}).

increased electron temperature and smearing of the Fermi distribution in the tip under illumination, whereas the local work function change is negligible.

FERs are also subject to the Stark effect caused by the electric field in the junction [17]. While the positions of the higher-order peaks are varied considerably by the Stark effect, the $n(n') = 1$ peak position is much less affected because it is determined largely by the image potential rather than the electric field in the junction. At larger gap distances the FER peaks are redshifted and their spacing becomes smaller because the potential gradient in the junction is gentler. These variations can be seen in the FER spectra with and without illumination [Fig. 1(a)];

the tip-surface distance is larger in the former case due to the plasmon-assisted process, resulting in the redshift and the smaller spacing of the FER peaks. Also, in Fig. 1(b), the FER peaks show similar variations as the incident power density increases. The Stark effect is also responsible for the deviation of the downshift value from the incident photon energy for the higher-order peaks in contrast to the $n' = 1$ peak. As illustrated in Fig. 4, the potential gradient in the junction at $V_{n'}$, is smaller than that at V_n, causing the different spacing of the FER levels. The Stark effect is dominated by the applied dc bias voltage, whereas the influence of the ac near-field oscillating at optical frequencies may be negligible as estimated for a nanoscale gap [34].
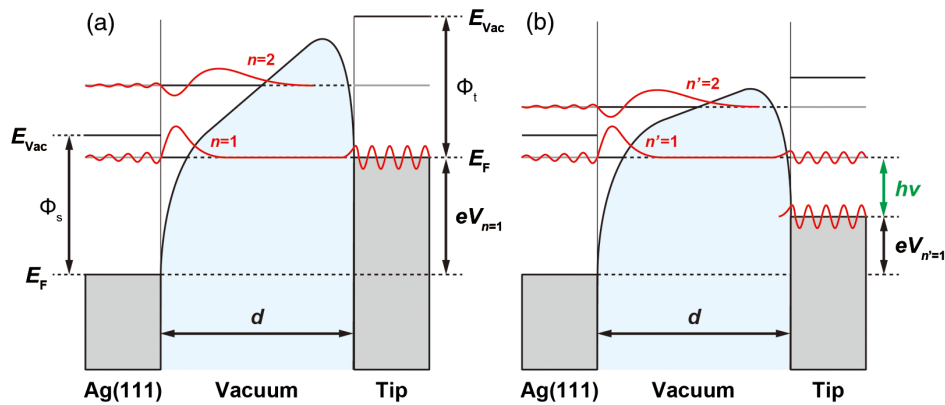

FIG. 4.   Schematic energy diagram of the Ag or Au tip-vacuum-Ag(111) surface junction (a) without and (b) with illumination. The blue shaded area represents the schematic potential in the junction. Fermi level (E_F), vacuum level ($E_{\rm vac}$), work function of the surface (tip) ($\Phi_{s(t)}$), sample bias (V_s), gap distance (d), index of the FERs [$n(n')$], FER voltage without (with) illumination [$V_{n(n')}$], schematic electron wave functions (red curves), incident photon energy ($h\nu$).

In summary, we demonstrated the plasmon-assisted resonant electron tunneling from a Ag or Au tip into FERs of the Ag(111) surface, which is induced by direct excitation of the junction with a focused cw laser. Our results revealed a novel electron transfer mechanism in a nanoscale plasmonic junction. Precise control of the cavity distance in the experiments combining STM with local optical excitation and detection is advantageous to examine the near-field properties particularly at the sub-nanometer scale, where quantum mechanical effects play a crucial role [35,36]. Moreover, the image potential states can be exploited to investigate excited electron dynamics [37,38]. Ultrashort optical excitation of plasmonic STM junctions therefore will provide an opportunity to trace the ultrafast electron dynamics at the nanoscale.

---

*Corresponding author.
kuma@fhi-berlin.mpg.de

[1] M. L. Brongersma, N. J. Halas, and P. Nordlander, Plasmon-induced hot carrier science and technology, Nat. Nanotechnol. **10,** 25 (2015).

[2] S. Grafström, Photoassisted scanning tunneling microscopy, J. Appl. Phys. **91,** 1717 (2002).

[3] B. Pettinger, P. Schambach, C. J. Villagómez, and N. Scott, Tip-enhanced Raman spectroscopy: Near-fields acting on a few molecules, Annu. Rev. Phys. Chem. **63,** 379 (2012).

[4] R. Zhang, Y. Zhang, Z. C. Dong, S. Jiang, C. Zhang, L. G. Chen, L. Zhang, Y. Liao, J. Aizpurua, Y. Luo, J. L. Yang, and J. G. Hou, Chemical mapping of a single molecule by plasmon-enhanced Raman scattering, Nature (London) **498,** 82 (2013).

[5] E. A. Pozzi, G. Goubert, N. Chiang, N. Jiang, C. T. Chapman, M. O. McAnally, A.-I. Henry, T. Seideman, G. C. Schatz, M. C. Hersam, and R. P. Van Duyne, Ultrahigh-vacuum tip-enhanced Raman spectroscopy, Chem. Rev. **117,** 4961 (2017).

[6] N. Tallarida, J. Lee, and V. A. Apkarian, Tip-enhanced Raman spectroscopy on the angstrom scale: Bare and CO-terminated Ag tips, ACS Nano **11,** 11393 (2017).

[7] J. Lee, S. M. Perdue, D. Whitmore, and V. A. Apkarian, Laser-induced scanning tunneling microscopy: Linear excitation of the junction plasmon, J. Chem. Phys. **133,** 104706 (2010).

[8] Y. Terada, S. Yoshida, O. Takeuchi, and H. Shigekawa, Real-space imaging of transient carrier dynamics by nanoscale pump–probe microscopy, Nat. Photonics **4,** 869 (2010).

[9] A. Dolocan, D. P. Acharya, P. Zahl, P. Sutter, and N. Camillone, III, Two-color ultrafast photoexcited scanning tunneling microscopy, J. Phys. Chem. C **115,** 10033 (2011).

[10] T. L. Cocker, V. Jelic, M. Gupta, S. J. Molesky, J. A. J. Burgess, G. De Los Reyes, L. V. Titova, Y. Y. Tsui, M. R. Freeman, and F. A. Hegmann, An ultrafast terahertz scanning tunnelling microscope, Nat. Photonics **7,** 620 (2013).

[11] K. Yoshioka, I. Katayama, Y. Minami, M. Kitajima, S. Yoshida, H. Shigekawa, and J. Takeda, Real-space coherent manipulation of electrons in a single tunnel junction by single-cycle terahertz electric fields, Nat. Photonics **10,** 762 (2016).

[12] T. L. Cocker, D. Peller, P. Yu, J. Repp, and R. Huber, Tracking the ultrafast motion of a single molecule by femtosecond orbital imaging, Nature (London) **539,** 263 (2016).

[13] S. Li, S. Chen, J. Li, R. Wu, and W. Ho, Joint Space-Time Coherent Vibration Driven Conformational Transitions in a Single Molecule, Phys. Rev. Lett. **119,** 176002 (2017).

[14] S. Dey, D. Mirell, A. R. Perez, J. Lee, and V. A. Apkarian, Nonlinear femtosecond laser induced scanning tunneling microscopy, J. Chem. Phys. **138,** 154202 (2013).

[15] S. W. Wu, N. Ogawa, and W. Ho, Atomic-scale coupling of photons to single-molecule junctions, Science **312,** 1362 (2006).

[16] S. W. Wu and W. Ho, Two-photon-induced hot-electron transfer to a single molecule in a scanning tunneling microscope, Phys. Rev. B **82,** 085444 (2010).

[17] G. Binnig, K. H. Frank, H. Fuchs, N. Garcia, B. Reihl, H. Rohrer, F. Salvan, and A. R. Williams, Tunneling Spectroscopy and Inverse Photoemission: Image and Field States, Phys. Rev. Lett. **55,** 991 (1985).

[18] R. S. Becker, J. A. Golovchenko, and B. S. Swartzentruber, Electron Interferometry at Crystal Surfaces, Phys. Rev. Lett. **55,** 987 (1985).

[19] J. Martínez-Blanco and S. Fölsch, Light emission from Ag(111) driven by inelastic tunneling in the field emission regime, J. Phys. Condens. Matter **27,** 255008 (2015).

[20] T. Kumagai, S. Liu, A. Shiotari, D. Baugh, S. Shaikhutdinov, and M. Wolf, Local electronic structure, work function, and line defect dynamics of ultrathin epitaxial ZnO layers on a Ag(111) surface, J. Phys. Condens. Matter **28,** 494003 (2016).

[21] See Supplemental Material at http://link.aps.org/supplemental/10.1103/PhysRevLett.121.226802 for FER spectra of the Ag tip-Ag(111) surface junction with 446 nm excitation and at a high incident power density, FER and STML spectra recorded under different tip conditions.

[22] P. B. Johnson and R. W. Christy, Optical constants of the noble metals, Phys. Rev. B **6,** 4370 (1972).

[23] J. Aizpurua, S. P. Apell, and R. Berndt, Role of tip shape in light emission from the scanning tunneling microscope, Phys. Rev. B **62,** 2065 (2000).

[24] M. I. Stockman, Nanofocusing of Optical Energy in Tapered Plasmonic Waveguides, Phys. Rev. Lett. **106,** 019901(E) (2011).

[25] C. Ropers, C. C. Neacsu, T. Elsaesser, M. Albrecht, M. B. Raschke, and C. Lienau, Grating-coupling of surface plasmons onto metallic tips: A nanoconfined light source, Nano Lett. **7,** 2784 (2007).

[26] T. Jung, Y. W. Mo, and F. J. Himpsel, Identification of Metals in Scanning Tunneling Microscopy via Image States, Phys. Rev. Lett. **74,** 1641 (1995).

[27] M. Pivetta, F. Patthey, M. Stengel, A. Baldereschi, and W.-D. Schneider, Local work function Moiré pattern on ultrathin ionic films: NaCl on Ag(100), Phys. Rev. B **72,** 115404 (2005).

[28] P. Ruffieux, K. Aït-Mansour, A. Bendounan, R. Fasel, L. Patthey, P. Gröning, and O. Gröning, Mapping the Electronic Surface Potential of Nanostructured Surfaces, Phys. Rev. Lett. **102,** 086807 (2009).

[29] K. Schouteden and C. Van Haesendonck, Quantum Confinement of Hot Image-Potential State Electrons, Phys. Rev. Lett. **103,** 266805 (2009).

[30] E. V. Chulkov, V. M. Silkina, and P. M. Echenique, Image potential states on metal surfaces: Binding energies and wave functions, Surf. Sci. **437,** 330 (1999).

[31] V. Kravtsov, S. Berweger, J. M. Atkin, and M. B. Raschke, Control of plasmon emission and dynamics at the transition from classical to quantum coupling, Nano Lett. **14,** 5270 (2014).

[32] H.-C. Ploigt, C. Brun, M. Pivetta, F. Patthey, and W.-D. Schneider, Local work function changes determined by field emission resonances: NaCl/Ag(100), Phys. Rev. B **76,** 195404 (2007).

[33] S. Stepanow, A. Mugarza, G. Ceballos, P. Gambardella, I. Aldazabal, A. G. Borisov, and A. Arnau, Localization, splitting, and mixing of field emission resonances induced by alkali metal clusters on Cu(100), Phys. Rev. B **83,** 115101 (2011).

[34] A. Stolz, J. Berthelot, M.-M. Mennemanteuil, G. C. des Francs, L. Markey, V. Meunier, and A. Bouhelier, Nonlinear photon-assisted tunneling transport in optical gap antennas, Nano Lett. **14,** 2330 (2014).

[35] W. Zhu, R. Esteban, A. G. Borisov, J. J. Baumberg, P. Nordlander, H. J. Lezec, J. Aizpurua, and K. B. Crozier, Quantum mechanical effects in plasmonic structures with subnanometre gaps, Nat. Commun. **7,** 11495 (2016).

[36] The junction distance during the FER measurements appeared to be larger than at least 1 nm, because the junction did not crash even if the tip approached the surface by 1 nm from a typical feedback setpoint of $V_s = 1$ V and $I_t = 0.1$ nA.

[37] M. Wolf, E. Knoesel, and T. Hertel, Ultrafast dynamics of electrons in image-potential states on clean and Xe-covered Cu(111), Phys. Rev. B **54,** R5295 (1996).

[38] U. Höfer, I. L. Shumay, Ch. Reuß, U. Thomann, W. Wallauer, and Th. Fauster, Time-resolved coherent photoelectron spectroscopy of quantized electronic states on metal surfaces, Science **277,** 1480 (1997).